RSC Sustainability

ROYAL SOCIETY OF CHEMISTRY

PAPER

View Article Online
View Journal

Cite this: DOI: 10.1039/d6su00025h

Ultrasonic decoating of solid oxide cell particles for raw material recycling

Carlo Kaiser * and Urs Alexander Peuker

With the expansion of hydrogen production capacities, solid oxide cells (SOCs) are becoming increasingly important. SOCs are multi-layer components which contain high concentrations of critical raw materials, including rare earth elements, making recycling crucial. Most published recycling approaches to date involve either manual labor or hydrometallurgical processes where harmful residues are produced. Ultrasonic decoating is a novel method that avoids these problems. A previous study showed that with ultrasonic decoating the perovskite layers on the air side of the SOCs can be selectively separated. However, this approach can be challenging due to the orientation dependence of the ultrasonic stress on the cells in combination with their mechanical fragility. To overcome this, this study investigates the ultrasonic decoating of SOC particles instead of whole cells. For this purpose, two cells with varying air sides are mechanically crushed and sieved, whereby the crushing behavior is investigated. The coarse particles are subsequently subjected to ultrasonic stress. Overall, the perovskites are selectively comminuted, enabling an initial concentrate to be obtained by crushing alone. Subsequent ultrasonic decoating improves the purity of both products, thereby increasing the recovery of the perovskites from the examined cells to 85% and 98%, respectively.

Received 14th January 2026
Accepted 9th March 2026

DOI: 10.1039/d6su00025h

rsc.li/rscsus

Sustainability spotlight

Developing efficient recycling routes for solid oxide cells (SOCs) is essential for reducing resource depletion and supporting a circular energy economy. This study demonstrates that combining mechanical crushing with ultrasonic decoating selectively detaches air-side layers, opening direct recycling pathways for all major SOC materials and avoiding the hazardous residues associated with hydrometallurgical methods. High recovery and purity directly contribute to SDG 12 (Responsible Consumption and Production) by keeping valuable resources in circulation and minimizing waste. Simultaneously, enhancing the recyclability of SOCs strengthens the sustainability of hydrogen technologies, thereby advancing SDG 7 (Affordable and Clean Energy) and SDG 9 (Industry, Innovation and Infrastructure). These results highlight the importance of innovative, low-impact recycling strategies in establishing robust clean energy systems.

Introduction

Water electrolyzers play a central role in the production of green hydrogen, a key element of a sustainable and climate-neutral energy future.[1] Among the electrolyzers that have been commercialized,[2] solid oxide electrolyzers (SOELs) stand out for their high electrical efficiency and the feasibility of their reversible operation as fuel cells.[3–5] However, the elevated operating temperature leads to accelerated material degradation, which in turn results in a relatively short lifetime of 2–3 years.[6,7] SOELs typically consist of repeating, stacked components, with the electrochemically active solid oxide cell (SOC) being the core component.

SOCs consist of microscopically thin layers that contain at least the fuel gas electrode, the electrolyte, and the air-side electrode for their functionality. There are different SOC designs depending on the type of mechanical support, also known as the substrate, of the cell. One of the most common designs is the fuel-electrode supported cell (FESC).[6,8] In FESCs, the layer adjacent to the substrate is the fuel gas electrode, followed by the electrolyte, the reaction barrier, the air-side electrode, and in some cases, a current collector layer. The state of the art (SoA) material for the substrate and the fuel gas electrode is a cermet consisting of yttria-stabilized zirconia (YSZ) and nickel.[9,10] YSZ is the oxygen ion conductor, which is also used as the electrolyte. The reaction barrier is typically composed of gadolinium-doped ceria (GDC).[8,10,11] Perovskites are commonly used for the air-side electrode and the respective current collector layer, while LSCF ($La_xSr_{1-x}Co_yFe_{1-y}O_{3-\delta}$) and LSC ($La_xSr_{1-x}CoO_{3-\delta}$) are SoA materials.[8,10,12]

The vast majority of elements utilized in SOCs are classified as either EU and US listed critical raw materials or strategic raw materials.[13,14] This criticality of these materials, combined with their short lifetimes and the increasing number of SOCs, makes a suitable recycling process essential. However, the development of appropriate and scalable end-of-life recycling processes

Institute of Mechanical Process Engineering and Mineral Processing, TU Bergakademie Freiberg, 09599, Freiberg, Germany. E-mail: Carlo.Kaiser@extern.tu-freiberg.de

is still in its early stages, with only a handful of published approaches.[15]

As part of the development of a holistic recycling scheme for SOELs, Kaiser, *et al.*[16] compiled and linked various recycling approaches for SOCs. They noted that most published recycling processes for SOCs involve two main steps: first, separating the perovskites; and second, processing the remaining ion conductors and nickel. There are two basic options for the processing of the nickel and ion conductors. The first option is the direct reutilization of the mixture in new SOCs as proposed by Sarner, *et al.*[17] The mixture can be reprocessed into new substrates by milling it to the specified particle size.[18–21] The alternative option involves additional separation steps to separate Ni from the ion conductors. Two approaches have already been investigated: the targeted leaching of Ni[22,23] and separation based on physical properties such as surface charge or magnetic susceptibility.[24] In both approaches, comminution is a necessary preliminary step to ensure the accessibility of the nickel for leaching and the complete liberation of the Ni-containing phase for mechanical separation. In addition to comminution, hydrothermal treatment can be used to disintegrate the YSZ structure to provide the required accessibility and liberation.[22,25]

For the separation of the perovskites, leaching-based strategies[18,19,26] or mechanical approaches[22,23,27] have been investigated.

Sarner, *et al.*[19] showed that leaching the perovskite LSCF with HCl at ambient temperature for 2 h showed promising results in terms regarding leaching efficiency, which reached up to 100%, and high selectivity for LSCF. They also examined direct oxalate precipitation, which produced a relatively pure La-oxalate (98.3%) suitable as a perovskite precursor. However, Sr, Co and Fe precipitated as mixed phases that, without additional pretreatment, are not suitable for SOC applications. Bruno *et al.*[26] developed and compared HCl-based ultrasound leaching strategies to selectively recover Co, La, and Sr from LSC in end-of-life SOCs. Their study evaluated different pretreatments, including milling and milling combined with thermal oxidation, as well as variations in acid concentrations and solid–liquid ratios. The highest recoveries of La, Sr, and Co, all above 96%, were obtained when ball-milled SOC powders were leached with 10 M HCl at 100 g L^{-1}. However, this condition also resulted in the dissolution of 68% of Ni, which reduced selectivity. In contrast, the highest purity was achieved through direct leaching without any pretreatment, using 1–5 M HCl at 200 g L^{-1}. Under these conditions, Ni leaching remained minimal, while the target metals still reached ~95% leaching with 5 M HCl and 91–92% with 1 M HCl, providing the most selective separation of La, Sr, and Co. Bruno *et al.*[26] also investigated oxalate precipitation as a downstream recovery step, which showed a clear trade-off between achieving high recovery and obtaining high purity. Leachates produced from 10 M HCl leaching of ball-milled samples resulted in the highest recoveries, with 85% Co and 82% La, although Sr reached only 15%, and the resulting precipitates had low purity due to unstable pH control. In contrast, oxalate precipitation after direct leaching with 1 M HCl produced much purer oxalates but at the cost of lower recoveries, with 42% Co, 93% La, and 33% Sr.

Overall, leaching-based approaches show promising leaching efficiencies, but subsequent precipitation remains a major challenge. In particular, the selective recovery of Sr and Co continues to limit the feasibility of closed-loop recycling. Furthermore, leaching processes typically require hazardous reagents that must be safely handled, disposed of, or recycled, which adds additional complexity to process implementation. These limitations highlight the need to consider alternative strategies that avoid chemical reagents altogether. Mechanical approaches offer such an alternative, as they rely on physical separation principles and therefore reduce or even eliminate the use of hazardous substances. For these reasons, mechanical routes warrant closer examination and, where technically feasible, should be preferred over leaching-based methods.

To date, two mechanical approaches to perovskite separation have been investigated. The first approach involves mechanical scraping followed by a surface cleaning step, which can be either polishing or acid cleaning, as described by Saffirio *et al.*[22] and Yenesew *et al.*,[23] respectively. This method has been shown to effectively remove the perovskites without leaving any residue. The polishing step can also be used to remove the underlying GDC reaction barrier. However, it should be noted that this process requires manual labor so far. Another mechanical option for the perovskite separation is ultrasonic decoating.[16] Kaiser *et al.*[27] investigated ultrasonic surface decoating and found that the perovskites can be selectively separated with high purity (>98%) using ultrasound, thus eliminating manual labor. Although the mechanical approaches investigated so far have shown promising results, they all face the challenge of automation, which is only possible to a limited extent.[16] End-of-life cells would come from the dismantling of electrolyzer stacks, and due to the low thickness and high brittleness of the cells, there is a high chance of the cells breaking, as already observed by Al Assadi *et al.*[28] However, since both mechanical approaches require the stress to be applied specifically to the perovskite layer, *i.e.*, the orientation of the cell is crucial, this could prevent or at least complicate the automatic application to broken cells.

In the past year, two alternative SOC recycling approaches have been proposed that begin with mechanical crushing of SOCs, followed by hydrometallurgical dissolution of most cell components.

As an initial step toward developing a complete recycling process, Völs *et al.*[29] evaluated the ability of various leaching agents to dissolve perovskites, nickel, and GDC from crushed SOC material. Among the tested reagents, hydrochloric acid achieved the highest leaching efficiencies. Although their study concentrates primarily on the leaching behavior, it also outlines potential downstream processing routes. The authors note that precipitation and liquid–liquid extraction may be applied for selected separations, but the chemical similarity and distribution of key elements across all cell layers ultimately require the separation of nearly all elements from one another after leaching. This necessity would result in a highly complex overall process. As shown in the studies discussed earlier in this manuscript on LSCF and LSC systems, even considerably simpler leachate compositions already pose significant

challenges for achieving clean and selective separation. These findings demonstrate that even for less complex systems, closed-loop recycling is difficult to realize, highlighting the significant challenges that must be expected for this approach.

Yenesew *et al.*[30] developed a recycling process in which nickel and LSC are recovered by dissolving the electrode materials in nitric acid, while YSZ remains as an insoluble residue that can be separated by centrifugation. Nickel is then selectively precipitated from the leachate through complexation with dimethylglyoxime, and the perovskite LSC is obtained by drying and thermally treating the remaining solution. Their study demonstrated that this combined mechanical and hydrometallurgical approach can recover NiO, YSZ, and LSC at commercial purity and can be scaled toward industrial application. However, the process has so far only been validated for LSC. In systems containing both LSC and LSCF, these perovskites would still need to be separated prior to reuse, otherwise the recovered material would be downcycled. Ongoing work aims to extend the method to other air electrode compositions and to improve separation purity, but the current results already highlight that even in comparatively simple systems, achieving fully selective recovery remains challenging.

Building on the limitations outlined above, these leaching-based processes, although potentially scalable, still require substantial quantities of hazardous chemicals, since roughly half of the cell materials must be fully dissolved to enable separation. This high degree of dissolution not only increases chemical consumption but also reinforces the environmental and operational burdens already previously highlighted, further underscoring why alternatives that avoid extensive use of chemical reagents should be considered wherever feasible.

This study investigates the use of ultrasonic decoating to separate perovskites from cell particles. The method, first introduced by Kaiser, *et al.*,[16] achieved promising initial results, recovering approximately 97% of the perovskite with a mass fraction exceeding 50%. The remaining cell materials were recovered with yields of up to 90%, offering the potential for reuse similar to the approach demonstrated by Sarner, *et al.*[17] However, these findings were based on a single tested cell and were not supported by systematic evaluation, meaning that the reproducibility of the process remained unverified at that stage. Compared with previously published mechanical strategies, ultrasonic decoating of particles offers several important advantages. It can process broken or fragmented cells, making it far more robust and better suited to real-world recycling streams, where intact components are rarely available. In addition, the process shows the potential to achieve high recovery rates without requiring precise geometric alignment or intact layer structures, which are the prerequisites for the other mechanical approaches. At the same time, ultrasonic decoating provides a compelling alternative to hydrometallurgical routes, as it operates purely mechanically, avoids hazardous chemicals, and preserves the chemical composition of the recovered materials. This opens the possibility for direct recycling and has the potential to reduce environmental impact and overall process costs compared with dissolution-based recycling methods.

In this study, the cells were preliminary crushed to prepare them for decoating. The resulting comminution product was sieved and analyzed for its composition. Coarse particles were then subjected to ultrasonic stress and the decoating of this size fraction was studied over time. The study concludes with an evaluation of the process as a whole, followed by a discussion of potential utilization pathways and subsequent processing steps for the products.

Material and methods

Cells

Two different cell types, each with a size of 10 cm × 10 cm, were examined. These were obtained from CeramTec/Forschungszentrum Jülich and Elcogen/Forschungszentrum Jülich. The cells are classified as waste material; they were never put into operation but are not functional and must therefore be treated as cell waste. The structure of the cells is shown in Fig. 1 and the composition is shown in Table 1. The cell components include NiO/YSZ cermet as the fuel-side electrode and substrate, a YSZ electrolyte, and GDC as the reaction barrier. The air-side electrode of cell 1 is composed of LSCF ($La_{0.58}Sr_{0.4}Co_{0.2}Fe_{0.8}O_{3-\delta}$). In cell 2, LSC ($La_{0.6}Sr_{0.4}CoO_{3-\delta}$) is used as the air side electrode and the current collector layer is composed of LSCF.

Material processing and characterization

Fig. 2 shows the SOC processing procedure. The SOC underwent preliminary crushing in a centrifugal ball mill (Pulverisette 6, Fritsch GmbH) until no larger cell fragments (>5 mm) remained, so that the particle size x of the cell fragments was suitable for ultrasonic decoating. For cell 1, this corresponded to 30 s of stress and for cell 2, 120 s of stress, both at level 10 intensity (700 rpm). YSZ balls with a diameter of 10 mm were selected as the grinding media and a YSZ bowl with a volume of 80 mL was selected as the grinding bowl. After crushing, the material was sieved at 1 mm, 315 μm, 200 μm, and 100 μm using a Retsch AS200 control "g" with an amplitude of 1.5 mm and a sieving time of 10 minutes. The sieve fraction at 315 μm was determined based on the cell thickness of the thinner cell. For particles larger than 315 μm, it can be assumed that most of the breakage occurred in a direction perpendicular to the layer structure. In contrast, smaller particles were also broken within the layered structure. Furthermore, a mesh size of 1 mm was

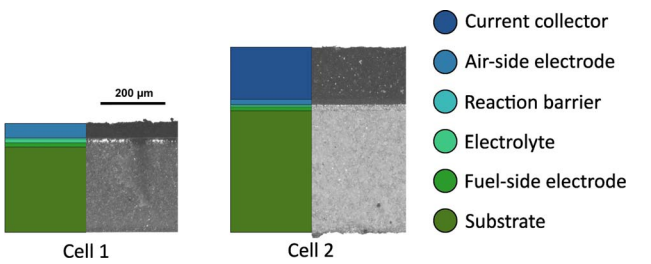

Fig. 1 Schematic structure and light microscope image of the cross-section of the SOC cell types.

Table 1 Bulk cell composition of cell 1 and cell 2

Material		Mass fraction in % Cell 1	Cell 2
Perovskites	LSCF	5.1 ± 0.1	10.9 ± 0.4
	LSC	—	2.4 ± 0.2
NiO		51.8 ± 0.7	43.6 ± 0.5
Ion conductors	YSZ and GDC	43.0 ± 0.7	43.0 ± 0.1

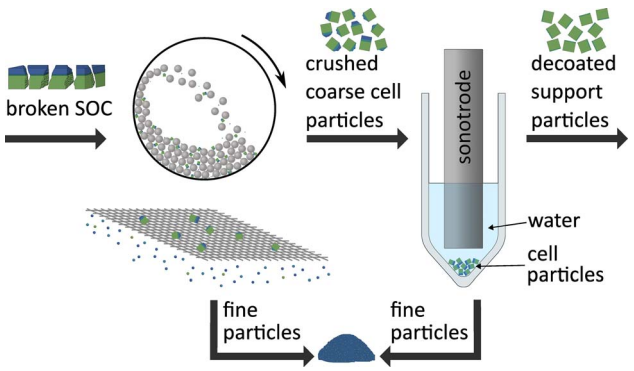

Fig. 2 Processing procedure for the SOC.

chosen to provide a quicker overview of the coarse particles, and two mesh sizes of 200 μm and 100 μm were added to investigate the accumulation of materials in the fines. In addition to sieve analysis, the particle size distribution of the two sieve fractions larger than 315 μm was examined using static image analysis, and the fraction ≤100 μm was analyzed using laser diffraction measurement (Mastersizer 3000, Malvern Instruments Ltd.). The content of perovskites, nickel and ionic conductors (YSZ, GDC) in all size fractions and in the original cell was determined using inductively coupled plasma optical emission spectroscopy (ICP-OES) (iCAP 6300, Thermo Fisher Scientific Inc; Waltham, United States). The perovskites and nickel oxide were dissolved in an inverse aqua regia solution by microwave-assisted dissolution (Multiwave 7000 Anton Paar GmbH, Graz, Austria).

The ultrasonic decoating setup is shown in Fig. 2 on the right. The cell particles were exposed to cavitating ultrasound in distilled water within a tube that was conically closed on one side. During exposure, the tapered tip ensured that the cell particles were guided back into the volume below the sonotrode. The sonotrode used was a Bandelin electronic UW 2200 with a maximum power draw of 200 W and a diameter of 12 mm. All particle size classes larger than 100 μm were used as input for decoating. After comminution and sieving the size classes coarser than 100 μm were mixed in their original mass ratio. The sample size used for each experiment was 200 mg in 5 ml of water. To study the decoating process, the cell particles were exposed to 160 W (as in Kaiser, *et al.*[27]) and analyzed after exposure times of 10 s, 20 s, 30 s and 40 s. Initial tests showed that this stress intensity achieved high decoating success while keeping particle breakage low. At lower stress intensities, the applied load did not overcome the adhesion between the coating and the substrate, or it did so only at a markedly reduced rate due to the insufficient magnitude of the local mechanical stress, as also demonstrated by Kaiser, *et al.*[27] when increasing the spacing between the sample and the sonotrode. Higher stress intensities increased bulk particle breakage and reduced selectivity, as the resulting fragmentation and splintering produced mixed material fragments instead of cleanly decoated particles. Stresses outside this range therefore do not yield meaningful selective decoating. Each decoating experiment was conducted three times. The suspension after decoating was decanted to separate the fine particles from the coarse support particles. The support particles were washed twice with 5 mL of distilled water each time and the resulting washing suspension was decanted and added to the decoating suspension containing the fine particles. The resulting suspension was dried at 80 °C for 16 h to obtain the fine particles. Due to the low amounts of fine particles from cell 1 after decoating, the three samples resulting from experiments under the same conditions were merged and analyzed together. The compositions of both concentrates were analyzed using ICP-OES. The particle size distribution of the fine particles was determined using laser diffraction analysis.

For simplicity, regarding composition this study distinguishes only two components c: the product P and the byproduct B. The byproduct consists of the ionic conductors and nickel, since most of the mass of the cell is a mixture of these materials. The perovskites represent the product.

The mass fraction of the perovskites was calculated from the measured perovskite elements obtained by ICP-OES, stoichiometrically accounting the unmeasured oxygen. The mass fraction of a component w_c, is the mass of the component m_c in relation to the total mass m:

$$w_c = \frac{m_c}{m} \quad (1)$$

The recovery of the component R_c in the respective concentrate can be determined as follows:

$$R_c = \frac{m_{c,\text{concentrate}}}{m_{c,\text{feed}}} \quad (2)$$

In this context, $m_{c,\text{concentrate}}$ stands for the mass of component P or B in the respective concentrate of the component and $m_{c,\text{feed}}$ for the mass of the component P or B in the feed of the considered process or process step.

Results and discussion

Crushing and sieving

As a preliminary step, the cells were crushed in the ball mill to prepare them in size for the decoating step. The particle size distribution originating from sieving of the crushed cells (1 and 2) is shown in Fig. 3a. For both cells, slightly more than 10% by mass is in the fines smaller than or equal to 100 μm. In the next two coarser particle size classes up to 315 μm, the value

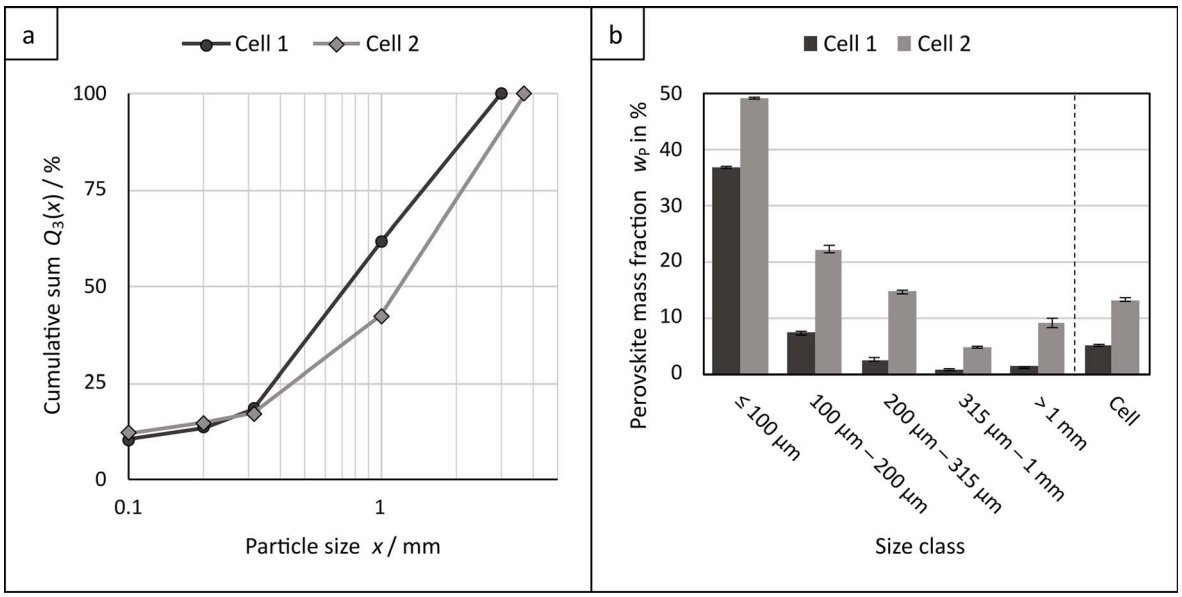

Fig. 3 (a) Particle size distribution resulting from the sieve analysis after the comminution (b) perovskite mass fraction in the particle size classes and the whole cell.

increases only slightly to approximately 18% (by mass), meaning that only a small amount of particles is crushed to that particle size. Up to 315 µm, the particle size distribution of the two cells is very similar. However, above 315 µm, a divergence in the curves of the two cells becomes apparent. Cell 1 shows just over 40% in the 315 µm to 1 mm fraction, while cell 2 shows only 25% in this same size class. Conversely, the coarsest fraction is just under 40% for cell 1 and just over 58% for cell 2. Cell 2 therefore has a higher proportion of coarse particles. In addition, the maximum particle size for cell 2 is coarser than for cell 1. However, for both cells the maximum particle size is less than 4 mm. The differences between the curves of the two cells can be attributed to the greater overall thickness of cell 2, which provides increased mechanical stability. Variations in the YSZ-to-NiO ratio within the substrate also affect mechanical robustness. Consequently, the higher YSZ content in the substrate of cell 2 is expected to further enhance its stability.

The perovskite mass fraction in the particle size classes and the entire cell for comparison is shown in Fig. 3b. The trend is consistent for both cell 1 and cell 2. There is a depletion of perovskites in the two coarsest particle size fractions, while there is an enrichment of perovskites in the two finest fractions. The most significant enrichment is observed in the finest fraction with a maximum size of 100 µm, where the perovskite content increases to almost 37% for cell 1 and to over 48% for cell 2, from an initial content in the feed material of about 5% and about 13%, respectively. The particle size class between 315 µm and 1 mm exhibits the lowest perovskite content.

The strong depletion of perovskites in particles between 315 µm and 1 mm, in contrast to the other particle size fractions, can be attributed to two main factors. Fig. 4 shows a cross-section of a coarse particle (size fraction > 1 mm) for both cell types. For both cells, the perovskite layers are more damaged at the edges than in the center of the particle. In the particle from cell 2, for instance, the perovskite layer at the edge has almost entirely been removed, increasing linearly in thickness up to approx. 800 µm from the edge. Beyond 800 µm, the layer structure remains almost constant and is comparable in thickness to that of the cell before comminution. For smaller particles, the distance between the center and the edge is shorter, resulting in less perovskite overall in a layered structure. Due to the short crushing time, the coarse particles were not subjected to sufficient stress to comminute or damage the central areas, which led to a larger amount of perovskites in a layer structure on the particles than in finer ones. On the other hand, Fig. 4 also shows that perovskites have settled everywhere on the surface of the particles. Since smaller particles have a larger surface area to volume ratio, more fine perovskite particle mass can settle there per unit volume. This leads to an increase in the perovskite content due to these adhering particles. To counteract this phenomenon, wet screening or washing

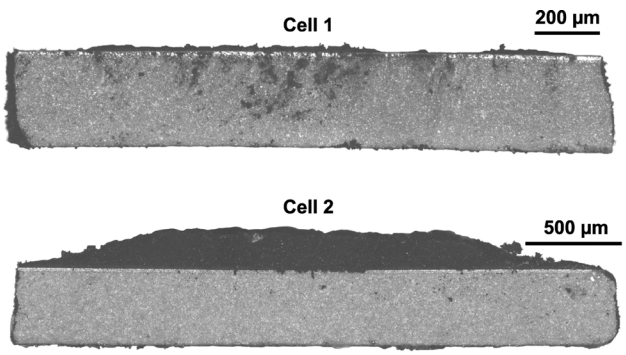

Fig. 4 Light microscope images of the cross-section through a coarse particle after crushing for cell 1 and cell 2.

methods could be used, as illustrated by the comparative images (Fig. S2 and S3) in the SI. These show that washing visibly reduces the fine particles adhering to the coarser particles, even though notable residues remain attached.

As shown in Fig. 3, the results indicate selective comminution of the perovskites, meaning that the perovskites are preferentially comminuted and accumulate in the fine fractions. Therefore, this fine fraction can be obtained as an initial product concentrate already after the preliminary crushing. In the product concentrates, 75% of the perovskites for cell 1 and 44% of the perovskites for cell 2 can already be recovered. However, the coarse particles still contain a significant amount of perovskite, especially considering that they make up almost 90% of the mass. Therefore, all fractions larger than 100 μm are subjected to particle decoating to recover the remaining perovskites.

No clear trend was observed in the ratio between NiO and ion conductors across the individual particle size classes (data in the SI). According to the manufacturer, the primary particle size of the substrates is in the single-digit micrometer range and below. However, since the particle size after comminution is significantly above these values, the cermet structure is still intergrown. As a result, the substrate exhibits a largely uniform ratio between NiO and ion conductors in the individual particles.

Ultrasonic decoating

The input to the decoating step was the cell particles >100 μm after preliminary crushing and sieving in a representative mass ratio as shown in Fig. 3a. The results are the average of the three individual decoating experiments at each time point, and the error bars represent the minimum and maximum values. The same applies to all decoated related results in subsequent figures. The recovery of perovskites from the decoating step over time is shown for cell 1 and cell 2 in Fig. 5a and b, respectively. For cell 1, approximately 82% of the perovskites in the corresponding concentrate are recovered in the first 10 s. In the following 10 s, only about 8% are added and then the process seems to almost stagnate at about 90%. The reason for the stagnation at about 90% may be due to several reasons. On the one hand, the sample quantity of fine particles obtained per experiment is rather small at about 2 to 3 mg. This sample may therefore be subject to fluctuations, especially in terms of losses, measurement uncertainties or feed compositions, which may affect the result. In addition, fine particles may settle on the surface and in the pores of the coarse support particles. Although attempts were made to counteract this effect by washing, the support particles still showed visible residues of perovskites even on the substrate after washing.

For cell 2, the highest increase in recovery of perovskites also occurs in the first 10 s. Thereafter, the slope decreases, but in contrast to cell 1, it does not stagnate but continues to increase until 40 s. This leads to the conclusion that decoating is not yet complete after 40 s and that longer sonication times would lead to a better recovery. Since two perovskites, LSCF and LSC, are used in cell 2, they are shown separately in Fig. 5b in addition to the total perovskites. The quantity of LSCF and LSC were estimated from the ICP-OES results based on stoichiometry. Since LSCF accounts for more than 80% of the perovskites content, the corresponding curve is comparable to that of the perovskites, with a shift toward higher recoveries. After 10 s, 67% of the LSCF was recovered and after 40 s, about 87% was recovered. In contrast, for LSC there is only a slight increase in the first 10 s to just 3% and then the curve is almost linear with a slightly higher slope until just over 30% of the LSC is recovered after 40 s. Since LSC represents the perovskite layer below

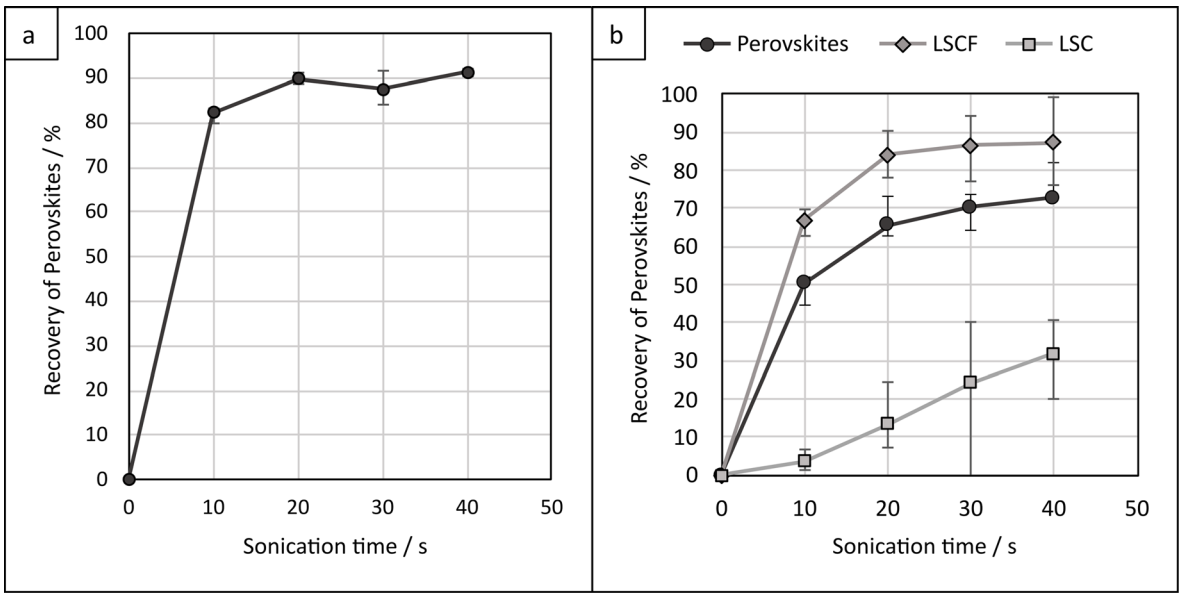

Fig. 5 Perovskite recovery over time during ultrasonic decoating for (a) cell 1 and (b) cell 2, with differentiation of the two perovskites used, LSC and LSCF.

the LSCF, the small increase in the beginning can be explained by the fact that the LSCF above the LSC must be removed first. Once LSCF is removed, LSC becomes accessible and begins to detach. The mechanical stability of the layers may also influence this recovery behavior. Considering the material densities of LSC and LSCF reported in the literature,[31–34] the combination of the layer thicknesses and measured masses indicates that, for this cell, the LSC layer exhibits a lower porosity than the LSCF layer. Given the similar mechanical properties of LSC and LSCF,[34] this lower porosity would correspond to higher mechanical stability and therefore aligns with the observed slower detachment of the LSC layer.

The curves for both cells show that most of the perovskites are detached at the beginning of the ultrasonic exposure, with a rapid decline thereafter. This observation suggests that the detachment from the air-side electrode near the interface to the reaction barrier requires a particularly high energy input, which is not applied in the stressing scenario applied here. This phenomenon was also previously observed by Kaiser, *et al.*[27]

Fig. 6 shows the Halbich diagram originating from mineral processing for cell 1 (Fig. 6a) and cell 2 (Fig. 6b) quantifying the decoating and separation. For both cells, the trend is that the perovskite mass fraction in the corresponding concentrate decreases with increasing recovery and thus increasing sonication time. As the perovskite concentrate samples for cell 1 had been merged, it was not possible to express the variation in the perovskite mass fraction in the product concentrate as minimum and maximum values derived from individual measurements. Instead, the limits of the individual product concentrate values were estimated based on the byproduct concentrate values and masses: for the minimum value it was assumed that all mass losses occurred in the product concentrate, and for the maximum value that all losses occurred in the byproduct concentrate. The same procedure was applied to estimate the individual recoveries. This approach, however, inherently overestimates the fluctuations in the individual measurements, as losses occur in both concentrates and the theoretical limit values are therefore not reached. Moreover, the very small sample quantities of only a few milligrams and the associated relative high mass losses, particularly for the product concentrate, can further amplify this overestimation. As a result, the error bars for the mass fraction appear disproportionately large and should be interpreted with caution, as they primarily reflect methodological limitations rather than true process variability. Conducting the experiments at a larger scale would substantially reduce these limitations, since mass losses would become small relative to the total sample mass and the product concentrates could be evaluated separately. This would allow direct determination of individual mass fractions and recoveries and would therefore provide a more reliable validation of the experimental results. An alternative way to estimate the fluctuations would have been to use the limit values of the combined sample, but this would likely underestimate the variability of the individual measurements. For this reason, the conservative overestimation approach was chosen.

For cell 1 (Fig. 6a), the perovskite mass fraction decreases rapidly from about 77% to about 53% as the recovery increases from about 82% to about 91%. As mentioned above, there is hardly any increase in recovery after 10 s ultrasonication, *i.e.* hardly any more perovskite is detached. However, since the perovskite mass fraction is reduced, this means that a higher proportion of byproduct is detached and contaminates the product concentrate. Therefore, the optimum balance between recovery and purity must be found here, depending on the purities required for reuse or for effective subsequent separation steps. Cell 2 (Fig. 6b) shows a slight decrease in perovskite mass fraction from about 74% to about 67% over the course of 40 s, with a significant improvement in recovery from about

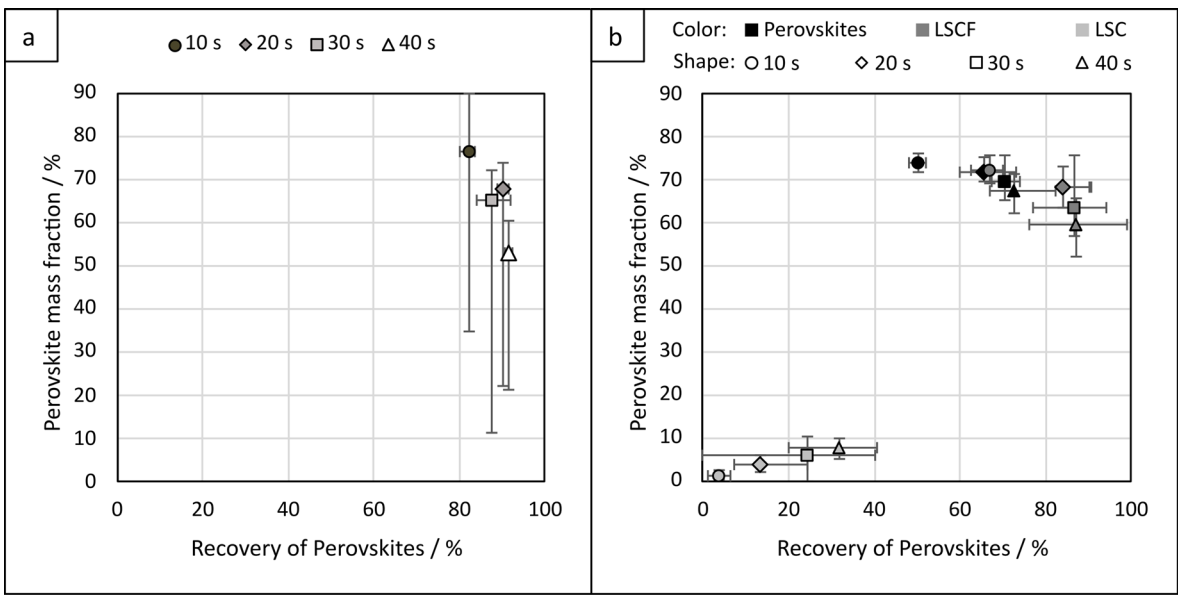

Fig. 6 Halbich diagram of the perovskites as a function of sonication time from the decoating step for (a) cell 1 and (b) cell 2.

50% to about 72%. As long as the value of recovery increases, the decoating process is incomplete and the amount of perovskite in the concentrate continues to rise, as mentioned above. For this reason, contamination of the perovskite concentrate increases slowly, as a large amount of perovskite continues to be detached. To gain a better insight into the decoating process, Fig. 6b additionally presents the perovskites LSCF and LSC separately. Even though the recovery of LSCF increases, the mass fraction of LSCF falls from about 72% to 59%, indicating that an increasing proportion of non-LSCF material is being removed and that the LSCF decoating process is slowly coming to an end. In contrast, the decoating of LSC has only just begun, as not only has recovery increased, but the mass fraction has also risen from approximately 1% to approximately 8%. This suggests that a longer decoating time would particularly favor the LSC yield. As LSC contains more cobalt than LSCF, it is considered as more valuable. Therefore, a longer exposure time and the associated higher LSC yield are worthwhile.

Process evaluation and reuse potential

In the preceding chapters, the two steps of selective preliminary comminution and decoating were evaluated independently. However, to evaluate the overall process, the final product concentrate, which is the combination of the product concentrates from both steps, and the remaining byproduct have now to be considered. Fig. 7 shows the Halbich diagrams for cell 1 and cell 2 for the process as a function of the sonication time. The 0 s point corresponds to the concentrate without a decoating step, which is the perovskite concentrate from the sieving at 100 μm. For cell 1 (Fig. 7a), both the recovery and the mass fraction of the perovskites in the product can be enhanced by decoating. The large fluctuations observed in the decoating experiments result from the error estimation applied to this step, as described previously, where the uncertainty can be substantially overestimated and must therefore be interpreted with caution. The recovery exhibits a notable improvement of up to more than 20 percentage points, while the mass fraction of perovskites in the concentrate increases slightly. The duration of the sonication time shows the same influence as for decoating in Fig. 6a. A short decoating time results in a concentrate with a slightly higher perovskite fraction, while a longer exposure time slightly increases the recovery at the expense of the purity of the product concentrate.

Fig. 7b shows for cell 2 as well a significant increase in the recovery and mass fraction of perovskites in the corresponding concentrate as a result of ultrasonic decoating. The recovery increases from about 44% to about 85% and the perovskite mass fraction can be increased from about 49% to about 57%. In the perovskite concentrate, the mass fraction of product in the product concentrate hardly changes (<1%) with different sonication times, while there is a significant increase in recovery from about 72% to 85%. This supports the assumption from the decoating evaluation that longer exposure probably has only a slightly negative effect on the composition of the perovskite concentrate but improves the recovery.

The perovskite concentrates exhibit a much higher perovskite content than the original cell but cannot be directly reused in a closed loop due to too high impurity content (NiO, YSZ and GDC). Therefore, further refinement is needed. One possibility is mechanical separation processes based on physical material properties, such as surface charge or magnetic susceptibility as analyzed and proposed by Ahn, *et al.*[24] Mechanical separation processes do not chemically alter the perovskites, and direct reuse could be an option. In addition, processing without hazardous substances is possible. However, mechanical separation processes have not yet been sufficiently researched in

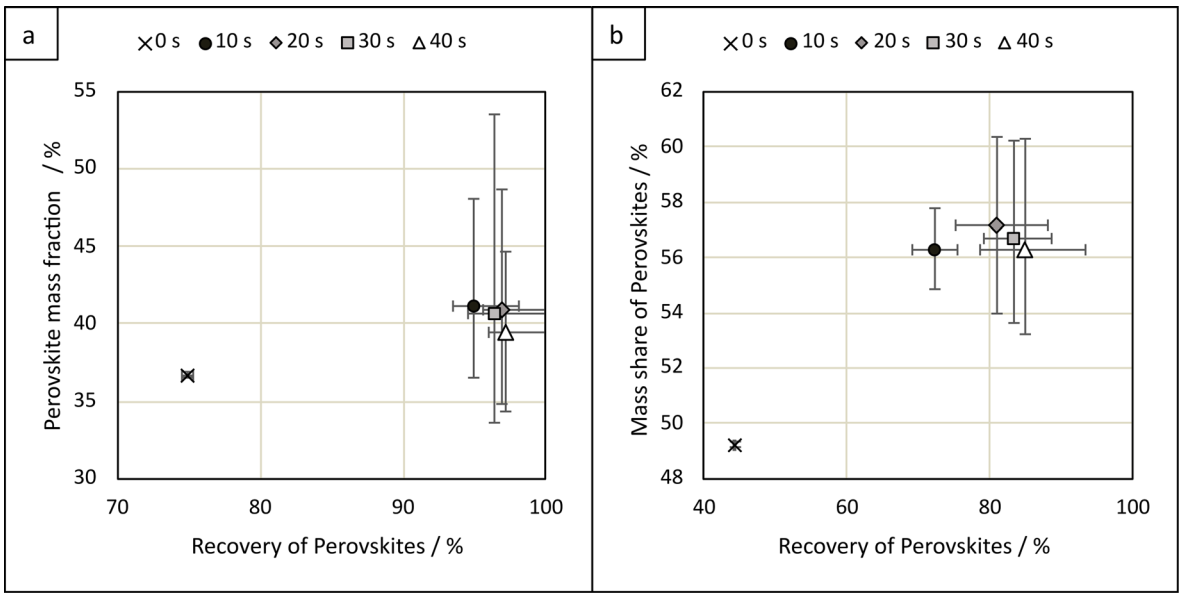

Fig. 7 Halbich diagram of the perovskites as a function of sonication time when combining the product concentrates after sieving and after decoating for (a) cell 1 and (b) cell 2.

SOC-related applications, and once purified material fractions can be recovered, their potential for reuse and their electrochemical performance will need to be thoroughly evaluated. Another option is the process presented by Yenesew, *et al.*[30] In contrast to the approach presented by Yenesew, *et al.*,[30] a concentrate is already available and thus a large part of the mass has already been separated. Therefore, the use of chemicals can be greatly reduced.

Fig. 8 shows the Halbich diagrams for the byproduct for cell 1 and cell 2 as a function of the sonication time. For both cells, the trend shows that the purity, the decrease of perovskite material respectively, of the byproduct concentrate can be increased by ultrasonic decoating. This means that the perovskites are selectively detached from the support particles. However, byproduct is also separated, so that the recovery from the byproduct decreases with increasing ultrasonic exposure. For cell 1, the contamination in the byproduct concentrate can be significantly reduced by ultrasonic decoating. However, it is observed that there is only a marginal increase in purity over the ultrasonic exposure duration ranging from 10 seconds to 40 seconds. Therefore, to maximize the recovery, a tradeoff must be found here as to when the byproduct concentrate has reached a sufficient purity for reuse. For cell 2, the greatest improvement in the byproduct purity is also achieved in the first 10 s of ultrasonic exposure from 92% to 97%. With continued exposure, a further improvement in purity to about 99% can be achieved in an almost linear progression, while the recovery decreases from over 91% to about 90%. Again, the purity required will depend on the specification of the reuse case.

Probably the best reuse option is the method proposed by Sarner, *et al.*,[17] which is to reuse the byproduct concentrate as substrate material for new SOCs. While purity requirements in the substrate are also important to ensure the longevity of the entire cell assembly, contamination in the substrate is considered to be the least critical compared to other layers.[27] The acceptable level of contamination still needs to be investigated. Should it be found that the perovskite contamination is still too high for direct reuse after decoating, or that the required duration of the decoating process results in too great a loss of byproduct, any remaining perovskite impurities in the material could be removed by leaching. Due to the previous mechanical reduction of perovskite content, it is expected that this can be achieved with shorter leaching times and lower amounts of acids than in Sarner, *et al.*[19]

Conclusions and outlook

This study investigated the application of ultrasonic decoating to cell particles for the selective removal of perovskites from broken SOCs. First, the cell fragments were coarsely crushed and sieved at 100 μm, enabling up to 75% of the perovskites to be enriched and recovered in the fine material. The coarse particles were then decoated using ultrasound to selectively remove remaining perovskites. More than 50% of the perovskites detached within the first 10 s of ultrasound application. Further stress increased the recovery but also led to increasing contamination of the perovskite product. In the case of the cell with two perovskite layers, the outer layer was detached first and as soon as the inner layer became accessible, its detachment began. An optimum balance must therefore be found between recovery and purity in ultrasonic decoating, as this can vary depending on the cell being examined, the materials used, and the number and thickness of the layers. This optimum will depend on the subsequent process steps and the associated energy consumption and purity requirements.

The overall process was evaluated by combining the perovskite concentrates after sieving and decoating to create one product, while analyzing the remaining support particles as

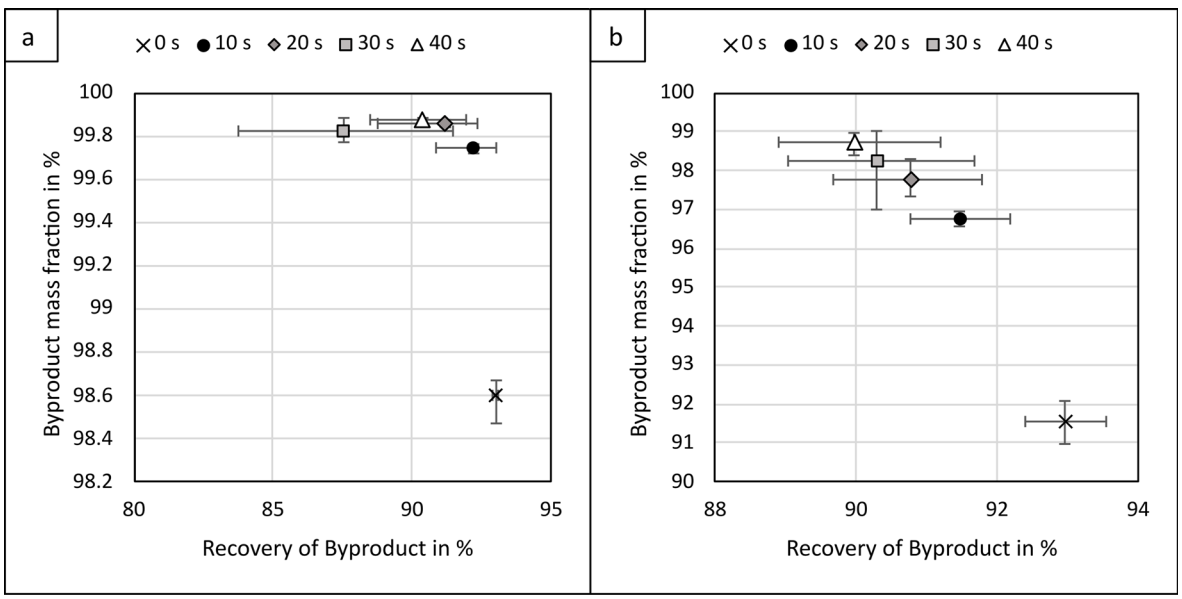

Fig. 8 Halbich diagram of the byproduct as a function of sonication time after decoating for (a) cell 1 and (b) cell 2.

a byproduct. This yielded product concentrates with perovskite contents of 40% and 57%, respectively, and recoveries of 98% and 85% for the cells under consideration. For the byproducts, purities of over 99% and recoveries of around 90% were achieved after ultrasonic decoating. Using ultrasonic decoating improved the composition of both the product and the byproduct. The recovery of the product increased significantly, while the recovery of the byproduct showed only a slight decrease. Therefore, ultrasonic decoating effectively led to selective separation of the perovskites and higher selectivity than comminution.

Further investigation is needed to implement a full recycling process for SOCs. This would involve integrating additional separation techniques or hydrometallurgical steps to maximize recovery and purity. Moreover, the impact of different comminution machines and principles, as well as the optimization of process parameters like sonotrode power, should be examined to improve efficiency and selectivity across the entire workflow.

Upscaling and automating the process remain essential steps toward industrial application. The small sample quantities used in this study (200 mg per experiment) can influence the results more strongly, as even minor handling losses represent a relatively large share of the total mass. Larger scale trials would reduce the relative impact of such losses and provide more robust performance data. However, scaling ultrasonic decoating is inherently challenging, because ultrasound propagation and especially cavitation behavior do not scale linearly with volume.

The energy consumption of this process would likely fall within the same order of magnitude as reported by Kaiser *et al.*,[27] who demonstrated that ultrasonic decoating exhibits a high mass specific energy demand. Scaling up would be beneficial, as larger volumes generally allow more favorable energy-to-mass ratios, yet ultrasonic decoating is still expected to remain on the higher end of energy demand within mechanical recycling. A meaningful assessment of whether this energy input can be justified by the benefits of the process can only be made once a scaled-up and more optimized configuration is available. Automating the current static setup would require considerable effort, which makes the transition toward a continuous process a more realistic and attractive development step. However, such a transition would substantially change both the scale and the process configuration, and sufficient residence time would still need to be ensured for effective decoating, introducing additional complexity in reactor design, flow control, and energy distribution. As a result, the overall energy consumption of a continuous system cannot be reliably evaluated at the current stage and must be addressed later in the development process, once the relevant design parameters are defined, and these factors must ultimately be resolved to enable reliable and energy-efficient operation at industrial scale.

Moreover, the materials examined in this study had not undergone real operation. Consequently, the effects of operational aging on the recycling process and on the formation of additional contaminants in the recovered concentrates remain unresolved. Aging processes in solid oxide cells can modify mechanical properties, introduce new phases and contaminants, and can thereby influence the purity of the resulting fractions and recycability.[35–37] Future research should include systematically aged cells to assess how operational degradation affects liberation behavior, separation efficiency, and contamination. Studies should also examine end-of-life cells dismantled from operating stacks to cover the entire spectrum of aging and potential sources of contamination for recycling under realistic conditions.

Author contributions

Carlo Kaiser: conceptualization, methodology, investigation, writing – original draft, writing – review & editing, visualization. Urs A. Peuker: funding acquisition, project administration, resources, supervision, writing – review & editing.

Conflicts of interest

There are no conflicts to declare.

Data availability

Supplementary information (SI) is available. See DOI: https://doi.org/10.1039/d6su00025h.

Acknowledgements

The authors thank the Forschungszentrum Jülich, for providing the solid oxide cells studied. The authors acknowledge the funding provided by the H2Giga-project ReNaRe, which was funded by the German Federal Ministry of Research, Technology and Space (BMFTR) (Grant No. 03HY111A). The authors would also like to thank Yvonne Volkmar for conducting the ICP-OES analysis and Annett Kästner for carrying out the laser diffraction measurements, as well as the remaining technical and scientific staff of the Institute of Mechanical Process Engineering and Mineral Processing. During the preparation of this work the authors used "DeepL Write" in order to improve the readability and language of the manuscript. After using this tool/service, the authors reviewed and edited the content as needed and take full responsibility for the content of the published article.

Notes and references

1 A. Kovač, M. Paranos and D. Marciuš, *Int. J. Hydrogen Energy*, 2021, **46**, 10016–10035.
2 IEA, *Global Hydrogen Review 2025*, IEA, Paris, 2025.
3 T. Capurso, M. Stefanizzi, M. Torresi and S. M. Camporeale, *Energy Convers. Manag.*, 2022, **251**, 114898.
4 M. Ji and J. Wang, *Int. J. Hydrogen Energy*, 2021, **46**, 38612–38635.
5 S. Sebbahi, N. Nabil, A. Alaoui-Belghiti, S. Laasri, S. Rachidi and A. Hajjaji, *Mater. Today Proc.*, 2022, **66**, 140–145.
6 A. Nechache and S. Hody, *Renew. Sustain. Energy Rev.*, 2021, **149**, 111322.

7 X. Sun, M. Chen, Y.-L. Liu, P. Hjalmarsson, S. D. Ebbesen, S. H. Jensen, M. B. Mogensen and P. V. Hendriksen, *J. Electrochem. Soc.*, 2013, **160**, F1074–F1080.
8 N. H. Menzler, D. Schäfer, N. Kruse, R. Peters and F. Kunz, *Ceram. Forum Int.*, 2023, **100**, 48–56.
9 S. Biswas, G. Kaur, G. Paul and S. Giddey, *Int. J. Hydrogen Energy*, 2023, **48**, 12541–12570.
10 S. E. Wolf, F. E. Winterhalder, V. Vibhu, L. G. J. (Bert) De Haart, O. Guillon, R.-A. Eichel and N. H. Menzler, *J. Mater. Chem. A*, 2023, **11**, 17977–18028.
11 J. Park, Y. Namgung, B. Singh, D. Shin, M. P. G. Hanantyo and S.-J. Song, *J. Alloys Compd.*, 2024, **976**, 173296.
12 D. Udomsilp, C. Lenser, O. Guillon and N. H. Menzler, *Energy Technol.*, 2021, **9**, 2001062.
13 European Commission, *Study on the Critical Raw Materials for the EU 2023 - Final Report*, European Commission, Luxembourg, 2023.
14 N. T. Nassar, D. Pineault, S. M. Allen, D. M. McCaffrey, A. J. Padilla, J. L. Brainard, M. Bayani, E. Shojaeddini, J. W. Ryter, S. Lincoln and E. Alonso, *Methodology and Technical Input for the 2025 U.S. List of Critical Minerals — Assessing the Potential Effects of Mineral Commodity Supply Chain Disruptions on the U.S. Economy*, U.S. Geological Survey, Reston, 2025.
15 M. Dragan, *Materials*, 2024, **17**, 6113.
16 C. Kaiser, S. Ahn, M. Brünner, D. Goes, J. Lastam, S.-O. Mongoljiibuu, S. Sarner, A. Specht, J. Fleischer, N. H. Menzler, M. Müller, M. Rudolph, B. Friedrich, O. Guillon, R. Schwaiger and U. A. Peuker, *Sustain. Mater. Technol.*, 2025, **45**, e01435.
17 S. Sarner, A. Schreiber, N. H. Menzler and O. Guillon, *Adv. Energy Mater.*, 2022, **12**, 2201805.
18 S. Sarner, N. H. Menzler, A. Hilgers and O. Guillon, *ECS Trans.*, 2023, **111**, 1369–1378.
19 S. Sarner, N. H. Menzler, J. Malzbender, M. Hilger, D. Sebold, A. Weber and O. Guillon, *Green Chem.*, 2025, **27**, 2252–2262.
20 S. Saffirio, S. Anelli, S. Pylypko, M. K. Rath, F. Smeacetto and S. Fiorilli, *Ceram. Int.*, 2024, **50**, 34472–34477.
21 G. G. Tutas, C. Timurkutluk, S. Onbilgin and B. Timurkutluk, *Resour. Conserv. Recycl.*, 2025, **212**, 107997.
22 S. Saffirio, S. Pylypko, S. Fiorot, I. Schiavi, S. Fiore, M. Santarelli, D. Ferrero, F. Smeacetto and S. Fiorilli, *Sustain. Mater. Technol.*, 2022, **33**, e00473.
23 G. T. Yenesew, E. Quarez, A. Le Gal La Salle, C. Nicollet and O. Joubert, *Resour. Conserv. Recycl.*, 2023, **190**, 106809.
24 S. Ahn, S. Patil and M. Rudolph, *Ind. Chem. Mater.*, 2024, **2**, 469–480.
25 M. Kamiya, Y. Mori, T. Kojima, R. Sasai and H. Itoh, *J. Mater. Cycles Waste Manag.*, 2007, **9**, 27–33.
26 M. Bruno, S. Saffirio, F. Smeacetto, S. Fiorilli and S. Fiore, *Batteries*, 2025, **11**, 124.
27 C. Kaiser, T. Buchwald and U. A. Peuker, *Green Chem.*, 2024, **26**, 960–967.
28 A. Al Assadi, D. Goes, S. Baazouzi, M. Staudacher, P. Malczyk, W. Kraus, F. Nägele, M. F. Huber, J. Fleischer, U. Peuker and K. P. Birke, *Resour. Conserv. Recycl. Adv.*, 2023, **19**, 200172.
29 P. Völs, T. Veiga Barreiros, A. D. Laplana, L. Sandig-Predzymirska and A. Charitos, *J. Sustain. Metall.*, 2025, **11**, 1766–1777.
30 G. T. Yenesew, C. Nicollet, E. Quarez, A. Le Gal La Salle and O. Joubert, *Sustain.*, 2025, **6**, 100110.
31 J. Prażuch, M. Pyzalski, D. Fernández González and T. Brylewski, *Materials*, 2024, **17**, 3791.
32 A. Möbius, D. Henriques and T. Markus, *J. Eur. Ceram. Soc.*, 2009, **29**, 2831–2839.
33 S. Kim, S. H. Kim, K. S. Lee, J. H. Yu, Y.-H. Seong and I. S. Han, *Ceram. Int.*, 2017, **43**, 1916–1921.
34 H. L. Lein, Ø. S. Andersen, P. E. Vullum, E. Lara-Curzio, R. Holmestad, M.-A. Einarsrud and T. Grande, *J. Solid State Electrochem.*, 2006, **10**, 635–642.
35 S. J. McPhail, S. Frangini, J. Laurencin, E. Effori, A. Abaza, A. K. Padinjarethil, A. Hagen, A. Léon, A. Brisse, D. Vladikova, B. Burdin, F. R. Bianchi, B. Bosio, P. Piccardo, R. Spotorno, H. Uchida, P. Polverino, E. A. Adinolfi, F. Postiglione, J. Lee, H. Moussaoui and J. Van Herle, *Electrochem. Sci. Adv.*, 2022, **2**, e2100024.
36 Y. Wang, W. Li, L. Ma, W. Li and X. Liu, *J. Mater. Sci. Technol.*, 2020, **55**, 35–55.
37 M. A. Hamayun, M. Gong, K. Park, M. Jo, Y. Bae, M. Kim, Y. Na, H.-T. Lim and J.-Y. Park, *J. Power Sources*, 2025, **658**, 238273.